Langmuir

ARTICLE

pubs.acs.org/Langmuir

Inkjet Metrology II: Resolved Effects of Ejection Frequency, Fluidic Pressure, and Droplet Number on Reproducible Drop-on-Demand Dispensing

R. Michael Verkouteren* and Jennifer R. Verkouteren

Surface and Microanalysis Science Division, Material Measurement Laboratory, National Institute of Standards and Technology, Gaithersburg, Maryland 20899, United States

S Supporting Information

ABSTRACT: We report highly reproducible gravimetric and optical measurements of microdroplets that lend insights into the fundamentals of drop-on-demand (DOD) printing. Baseline fluidic pressure within the DOD dispenser was controlled to within 0.02 hPa, enabling long-term stability in dispensed droplet mass with observed variations near 1% (RSD) for isobutanol. The gravimetric measurements were sensitive enough to detect and avoid unwanted effects from air bubbles within the dispenser. The gravimetric and optical velocity measurements enabled consistent determination of droplet kinetic energy that governed baseline behavior across the operational variables. Mass and velocity were influenced in a nonlinear manner by the frequency of droplet ejection, the fluidic pressure within the dispensing device, and the number of droplets dispensed in a burst. Resolved effects were attributable to several possible mechanisms including acoustic resonances, energy partitioning from systematic orifice refill dynamics, pressure wavelets created within the dispenser cavity during "first-drop" formation, and residual ring-down after last-drop emergence.

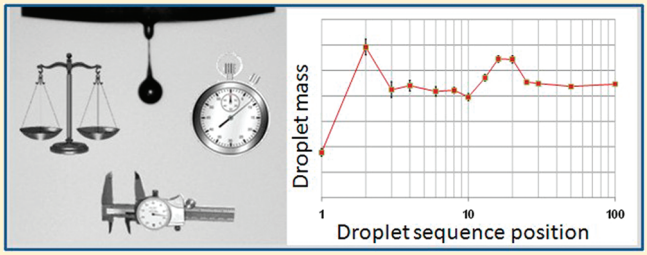

INTRODUCTION

Inkjet dispensing has been reported across diverse nanofabrication applications, including microfluidic systems,[1] drug-eluting stents,[2] photovoltaic arrays,[3] tissue engineering,[4] and graphene electronics.[5] Such applications require quantitative and spatially accurate deposition to ensure reproducible feature size, functionality, and analytical accuracy, but measurement and control over dispensed aliquot mass have been significant challenges. Droplet size measurements have typically employed optical and fluorescent methods, where limitations in resolution can translate to a 10% uncertainty in volume and mass. A further challenge has been described as the "first drop problem", where the first several droplets dispensed from a drop-on-demand (DOD) device can be significantly different in mass, velocity, and trajectory from subsequent droplets emerging during establishment of steady-state ejection conditions.[6−8] When dispensing droplets in small bursts, characterization of these "first droplets" may be critically important to the success of the application.

Commercial DOD inkjet dispensers operate by either piezoelectric deformation, electrostatic pull, or thermal transduction, and the dynamics of liquid jets and microdroplet generation are well described in the literature.[9−12] The diameters of the droplets produced are roughly equivalent to the diameters of the orifices from which they emerge, but other factors are also important.[13−15] These include the driving waveform, the droplet ejection frequency, the fluidic pressure in the fluid cavity, the orifice surface condition, and the rheological properties of the dispensed fluid. Practical issues such as particle entrapment and the growth of bubbles within the acoustic cavity of a piezoelectric transducer (PZT) have been identified as long-standing challenges to the quality of inkjet dispensing. Control over the dispensing process involves keeping operational conditions constant, but little quantitative information is available regarding the sensitivity of droplet size to changes in these conditions, especially when the effects occur below the level of measurement resolution. Recently, we reported on gravimetric methods that enabled studies on the metrology of picoliter dispensing at high accuracy and precision levels.[16] Briefly, a known number of droplets within a discrete burst or a series of bursts are dispensed into a partially filled capsule positioned on a submicrogram balance. The total dispensed mass, after a correction for baseline fluid evaporation from the capsule, is converted to an average mass per droplet. For large burst sizes, where "first-drop" effects are highly diluted, combined relative uncertainty in droplet mass is near 1%, while analytical repeatability is typically <0.5%. Because mass is measured directly, the shape of the droplets dispensed is unimportant, so the gravimetric method provides strong traceability to the Systeme Internationale (SI) with uncertainties significantly lower than those achievable through optical methods alone. Here, we use this gravimetric method coupled with advanced optical measurements to systematically

Received: May 9, 2011
Revised: June 11, 2011
Published: June 13, 2011

ACS Publications This article not subject to U.S. Copyright. Published 2011 by the American Chemical Society

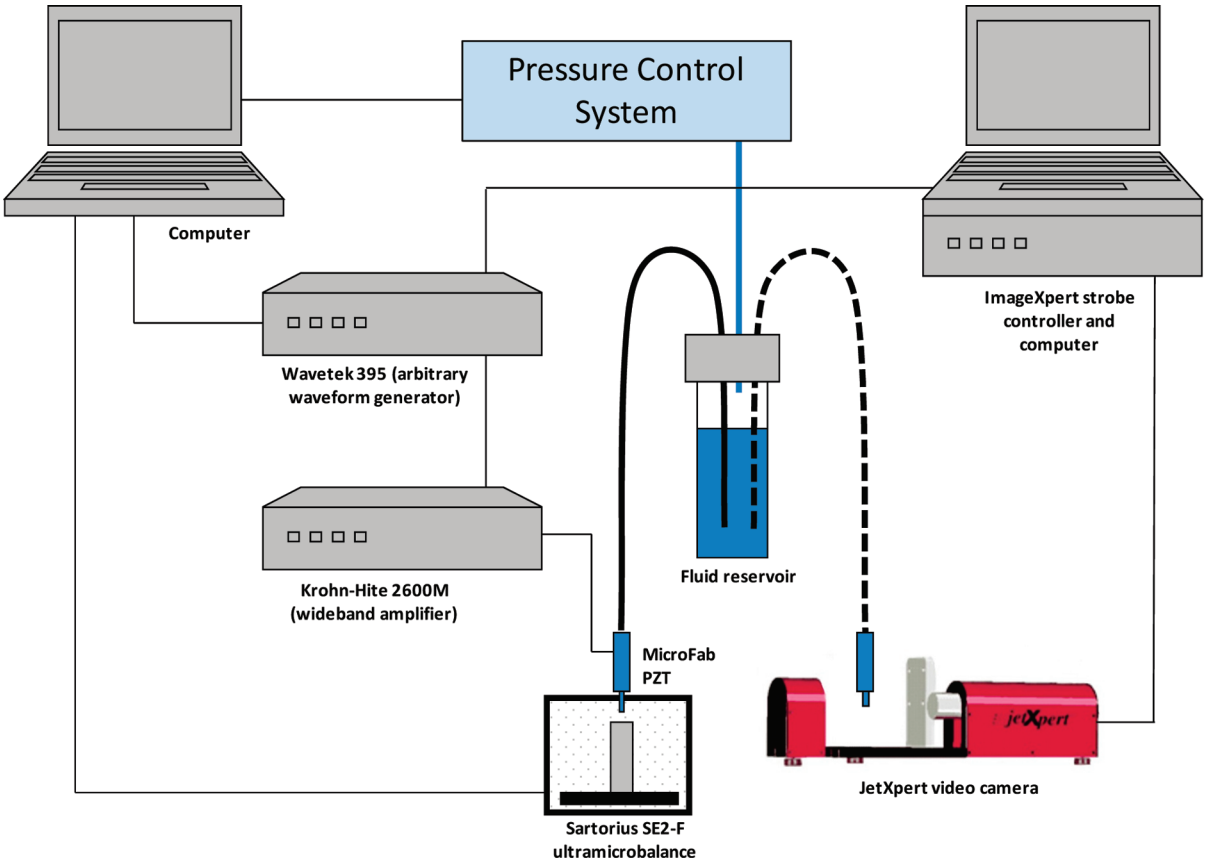

Figure 1. System for drop-on-demand generation of microdrops and gravimetric/optical characterizations. To move precisely between the balance and camera, the PZT device and fluid reservoir were mounted together on an $x-y-z$ stage and rotating armature (not shown). The pressure control system for the reservoir headspace is shown in Supporting Information (I).

investigate the sensitivity of droplet mass and velocity to three operational factors: ejection frequency, fluidic pressure, and burst size. The effects of bubble growth within the PZT device were also observed but were not systematically studied.

EXPERIMENTAL SECTION

Droplet Dispense and Characterization System. All work was performed at the National Institute of Standards and Technology (NIST) within the Advanced Measurement Laboratory complex, in which room temperature and relative humidity are specified to within 0.25 °C and 5%, respectively. A specialized DOD system was constructed from the following components mounted within a fume hood on an optical bench (Figure 1): a PZT inkjet device (MJ-AB-01-50, MicroFab Technologies, Plano, TX) was driven by a waveform generator (Wavetek 395) amplified by a wideband amplifier (Krohn-Hite 7600M). (Certain commercial equipment, instruments, or materials are identified in this document. Such identification does not imply recommendation or endorsement by the National Institute of Standards and Technology, nor does it imply that the products identified are necessarily the best available for the purpose.) A fluid reservoir was mounted so that the fluid level could be maintained at a constant height above the PZT device. The headspace pressure was digitally controlled through a pressure/vacuum regulator (MKS Instruments model PC90, 133 kPa full-scale, 50 sccm maximum flow, downstream control) using feedback from a differential manometer system referenced to ambient barometric pressure (MKS Baratron, model 698A, 133 kPa full-scale with 0.001 kPa resolution, powered through an MKS model 270B signal conditioner). See Supporting Information (I) for further description. An $x-y-z$ stage mounted on a rotatable armature was used to position the inkjet device precisely for either gravimetric or optical droplet characterizations without changing dispensing conditions.

The gravimetric system, described previously,[16] was modified as follows. Droplets were dispensed into a weighing capsule (Elemental Microanalysis Ltd., 20 mm (height) × 8 mm (diam) smooth-wall tin cylinder) already containing about 100 mg of the fluid being dispensed. This capsule was positioned on the weighing pan of a microbalance (Sartorius model SE2-F), with the pan and capsule enclosed in a cylindrical aluminum chamber (3 cm × 3 cm). This chamber had a 2 mm diameter hole centered about 2 mm above the top of the capsule to accommodate the tip of the PZT device. The chamber provided a static air space where steady-state evaporation from the capsule was quickly achieved. RS232-encoded data were captured directly into Microsoft Excel using WinWedge software v.3.4 (TALtech).

Optical measurements were performed using a JetXpert video system (ImageXpert Inc., Nashua, NH), which has an integrated high-power LED strobe capable of pulse widths down to 250 ns allowing image capture of individual droplets in flight. Additionally, double pulses separated by times down to 800 ns enabled measurement of near-instantaneous velocities at several discrete positions below the orifice. Camera resolution could be adjusted between 1.1 and 6.1 μm per pixel within a field of view of 1024 × 768 pixels, with dimensional calibration effected through a standard slit artifact. The JetXpert system was triggered through synchronized TTL signals from the Wavetek 395, which was programmed to generate multiple (1−2000) bursts of unipolar pulses (each burst numbering anywhere between 1 and 20 000 pulses) at frequencies achievable with our PZT device (2.5 Hz to 24 kHz). A 400 ms delay

between bursts allowed quenching of acoustic resonance effects. This system enabled imaging of droplet bursts including optical comparison of first and subsequent droplet formation characteristics.

Selection of Operational Dispense Conditions. While strategies exist for setting operational variables,[17−19] we describe some practical considerations associated with this study. One goal was to collect and compare droplet mass and velocity data across a wide range of ejection frequencies. A fixed set of operating conditions was identified that would produce adequate droplets measurable by each technique across the tested ejection frequencies. Operational variables in DOD printing that affect droplet size and velocity include the rheological properties of the fluid ejected, fluid contamination with particles and gases, the characteristics of the driving waveform, the fluidic pressure, and the diameter and surface condition of the orifice. Operating variables are discussed in turn.

Orifice. Orifice diameter and condition were fixed in this study. Only one device was used, which was cleansed each day with high-purity acetone, mild abrasion, and ultrasonic agitation, preventing formation of scale that otherwise would influence the wettability of surfaces surrounding the orifice. Before use, the suitable condition of the orifice was verified by optical microscopy.

Fluid Rheology. While we report data for isobutanol (IBA), which has rheological properties well-suited for DOD printing, we have had success with printing other fluids and expect results reported here to be applicable over a wide range of solutions on comparably equipped DOD printers. For example, we dispensed droplets of the explosive 1,3,5-trinitroperhydro-1,3,5-triazine (RDX) in isopropanol (100 mg/L) on a modified MicroFab print station with a mass reproducibility of 0.38% (RSD, $n = 144$) across 42 h (see Supporting Information (II)). Aqueous solutions of ammonium nitrate, a challenging DOD fluid, have been dispensed at low ejection frequencies (<500 Hz) and in small bursts (<50 droplets) at higher ejection frequencies where mass uncertainties were ∼5%.

Fluid Contamination. We found that the presence of small air bubbles in the PZT device, invisible but sometimes evidenced by the upward drift of nonoccluding bubbles onto the walls of the fluid supply line, would cause a significant increase in dispensed droplet size presumably from unwanted acoustic reflections.[20] To prepare our fluids, particles were first removed by filtering through a 0.45 μm nylon filter (Millipore HPF Millex-HN). This caused aeration of the fluid and the risk of bubble growth by cavitation during acoustic cycling,[21] which could be detected through a steady rise in dispensed droplet mass. To minimize (but not completely eliminate) this risk, we allowed our fluid to outgas under a slight vacuum for 24 h before usage.[22] We also observed that air could be entrained in the PZT device when purged too forcefully with fluid. When droplet size was greater than 1% of our expectation, the PZT device was slowly evacuated, refilled, and retested.

Fluidic Pressure. The baseline pressure of the fluid inside the PZT nozzle cavity was controlled through static head level and regulation of reservoir headspace pressure and was determined through eq 1:

$$\Delta = \delta + hg\rho \tag{1}$$

where Δ is the baseline fluidic pressure (in hPa) in the PZT device, δ is the differential gas pressure (in hPa) between the reservoir headspace and ambient room pressure, h is the vertical distance (in cm) from the nozzle tip to the fluid level in the reservoir, g is the gravitational acceleration constant (9.81 m/s^2), and ρ is the density (in kg/m^3) of the fluid at the ambient temperature. The relationship was validated in a separate study by changing the values of δ and h and plotting droplet size versus the fluidic pressure (see Supporting Information (III)).

Driving Waveform. The droplet formation process was monitored through the JetXpert imaging system as the waveform for the dispensing device was adjusted. We used a trapezoidal waveform defined by five parameters: baseline voltage, rise time, dwell time, driving voltage, and fall time. Baseline voltage was set to 0 V, and rise and fall times were both set to 4 μs. Values for dwell time and driving voltage were varied, starting with 15 μs and 30 V, respectively. This initial dwell time was calculated through eq 2:

$$t_{\text{dwell}} + \frac{t_{\text{rise}} + t_{\text{fall}}}{2} = \frac{L}{c} \tag{2}$$

where L is the total length of the capillary (nominally 22 mm), and c is the effective speed of sound in the fluid.[23] For IBA within a capillary, the value of c was expected to be somewhat less than 1193 m/s, which is the value at 23 °C in bulk IBA.[24] However, a 15 μs dwell time caused an ejection process too energetic for our purposes at frequencies above 3000 Hz, leading to unsuitable satellite droplet formations that prevented accurate measurements of droplet velocities. Instead, we used 34 μs, a harmonic pulse-width at 2 L/c that resulted in a less energetic and simpler droplet formation process. Shown in Figure 2 is an idealized depiction of acoustic wave propagation in a DOD dispensing device containing an open-ended capillary and an annular PZT positioned near the middle of the capillary. The compression pulse from the initial PZT expansion is in the primary resonance position at 1 $L/c + t_o$, and a PZT compression at this time would amplify the pulse resulting in a droplet (at 1.5 $L/c + t_o$) with maximal velocity. If PZT compression is delayed until 2 $L/c + t_o$ (as shown in the figure), two crossing compression pulses from the initial PZT expansion are in position to be amplified. This results in less energetic droplet formation (at 2.5 $L/c + t_o$) that suppresses formation of undesired satellites. Residual acoustic waves continue to propagate, where compression waves traveling toward the orifice occur with a periodicity of 3 L/c. Figure 2 was inspired by a similar illustration in Bogy and Talke[17] where their contraction pulse occurred at $t_0 + 1L/c$.

Once the dwell time was established, reservoir head pressure and driving voltage were adjusted to maximize droplet velocity while avoiding long-lived (>400 μs) satellites that would otherwise interfere with the optical measurements. A set of conditions was found that satisfied all of our requirements. The fluidic head was fixed at −2.0 hPa by maintaining a static head level of 12.7 cm and a differential reservoir headspace pressure of −12.0 hPa. The trapezoidal waveform had the following characteristics: 36.0 V pulse height, 34.0 μs pulse width, 4.0 μs rise and fall times, and could produce droplets of IBA across frequencies between 2.5 Hz and 24 kHz at velocities greater than 1 m/s.

Measurements. *Droplet Velocity.* Because of variations in droplet formation, satellite assimilation, and subsequent oscillations at different ejection frequencies, our measurement of droplet velocity occurred 2.0 mm below the orifice. At this distance, all droplet formation effects had been quenched, and droplet aspect ratios were measured between 0.97 and 1.0. Using the JetXpert system, a double pulse (each 500 ns in duration) was generated that back-illuminated a droplet-in-flight before and after vertical travel of about 100 μm in the 2.0 mm region. To calculate velocity, the distance between the centers of the two droplet images was divided by the time set between the LED pulses. For some ejection frequencies greater than 4000 Hz where double pulses resulted in image overlaps with droplet neighbors in flight, another method was used. A single pulse was used to back-illuminate two neighbor droplets, and the distance between their centers was divided by the ejection period to determine velocity. Over the course of several days, these measurements were repeated at least 10 times to arrive at an average velocity and imprecision for each operating condition. We also estimated velocity attenuation due to air resistance by measuring velocities of a 500 Hz droplet stream at various distances from the orifice (see Supporting Information (IV)). The trend was linear between 0.5 mm and 2.0 mm, and at the 2.0 mm position, the velocity of a typical droplet was about 80% of the extrapolated value at the orifice. Because this factor was expected to affect all droplets proportionally and not influence the observed trends, we did not apply a correction for air resistance to the velocity measured.

Gravimetry. Gravimetric methods have been reported previously.[16] We used a weighing interval of 9.95 s, which avoided synchronization effects with the internal refresh rate of the microbalance. Each day, the

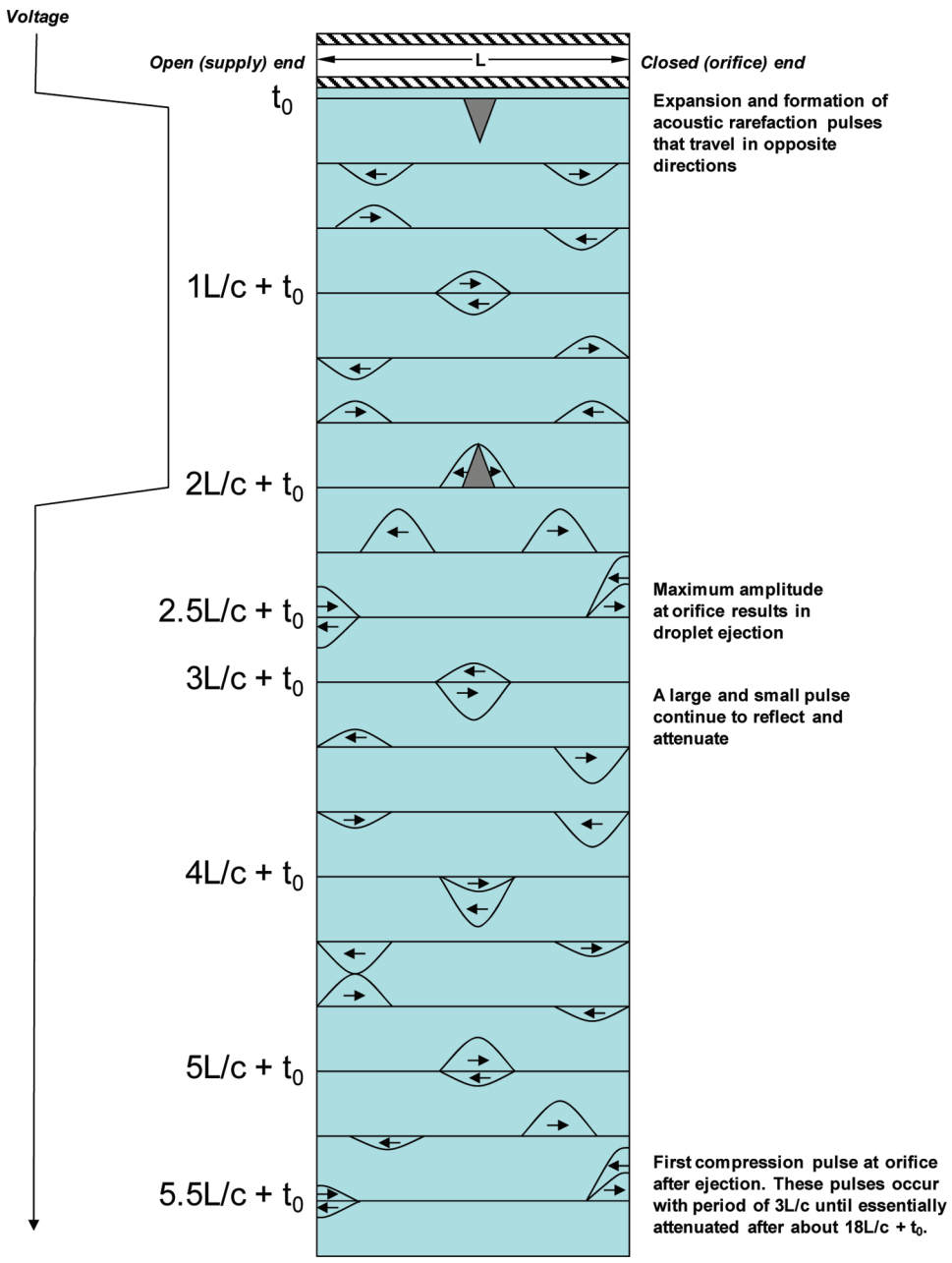

Figure 2. Idealized schematic of acoustic wave propagation in a DOD dispensing device.

balance was calibrated using internal weights verified with a set of SI-traceable standard weights. In characterizing the ejection frequency profile for IBA from 2.5 Hz to 24 kHz, the burst method was used. Results were determined through eq 3:

$$m = \frac{[M_2 - M_1]_\tau}{N} \tag{3}$$

where m is the average mass of a single droplet, N is the total number of droplets deposited (20 000, except at 10 Hz where 5000 droplets were delivered), and M_1 and M_2 are extrapolated balance readings of the evaporation trend, before and after ejection respectively, at time τ. We defined time τ as the point halfway between the last stable differential evaporation reading before ejection and the first stable differential evaporation reading after ejection. The burst method was also used for characterizing droplet mass sensitivity to fluidic pressure.

The pulsed burst method was used to characterize droplet mass sensitivity to burst size. Nineteen burst sizes, from 1 to 20 000 droplets (Table 1), were measured at 500, 5556, and 20 kHz. The dispense system was programmed to eject one of these bursts at each trigger signal, and a known number of trigger signals separated by 400 ms delay times was transmitted until the total mass of the droplets dispensed was greater than the minimal weight required by the specification of the microbalance. Burst mass was determined through eq 3 where m was the mass per burst and N was the number of bursts elicited by the program script.

Droplet Mass and Velocity versus Ejection Frequency. We measured droplet masses and velocities across ejection frequencies from 2.5 Hz to 24 kHz using a single trapezoidal driving waveform and constant operating conditions. The static head and reservoir headspace pressures were set at 12.7 cm IBA and −12.00 hPa, respectively, which corresponded to a total fluidic head pressure of −2.0 hPa in the PZT device.

Table 1. Drop-on-Demand Design

droplets per trigger	triggers	total number of droplets	dispense duration (s) 500 Hz	5556 Hz	20 kHz
20 000	1	20 000	40.0	3.6	1.0
10 000	2	20 000	40.4	4.0	1.4
5000	4	20 000	41.2	4.8	2.2
1000	10	10 000	23.6	5.4	4.1
500	20	10 000	27.6	9.4	8.1
100	50	5000	29.6	20.5	19.9
50	100	5000	49.6	40.5	39.9
30	200	6000	91.6	80.7	79.9
25	200	5000	89.6	80.5	79.9
20	300	6000	131.6	120.7	119.9
16	500	8000	215.6	201.0	200.0
13	500	6500	212.6	200.8	199.9
10	500	5000	209.6	200.5	199.9
8	1000	8000	415.6	401.0	400.0
6	1000	6000	411.6	400.7	399.9
4	1500	6000	611.6	600.7	599.9
3	2000	6000	811.6	800.7	799.9
2	2000	4000	807.6	800.3	799.8
1	2000	2000	803.6	800.0	799.7

At this condition, droplet velocity was maximized. The initial selection of 40 ejection frequencies within the range was uniform, and each was measured in random order. As the profile emerged, we filled in measurements that revealed fine-structure. Most fine-structure was delineated after 172 individual measurements of droplet mass and velocity, and several frequencies representing resonance maxima, minima, midpoints, and transitional and quiescent regions were selected for replicated measurements to determine reproducibility under those conditions.

Droplet Mass and Velocity versus Fluidic Pressure. We measured the average IBA droplet mass and velocity dispensed in a 20 000 drop burst across seven levels of differential fluidic pressure (measured against atmospheric pressure) at four ejection frequencies: 20 kHz, 5556 Hz, 500 Hz, and 10 Hz. The fluidic pressure in the PZT device was varied by adjusting the reservoir headspace pressure; static head was held constant at 12.7 cm IBA. Each measurement was replicated three times in random order for a total of 168 mass and velocity determinations. Formation of droplets was not possible beyond the fluidic pressure end points of −15.1 hPa and +0.7 hPa. Air would be drawn into the orifice at lower pressures, and fluid would ooze out of the orifice at higher pressures.

Average and Differential Droplet Mass versus Burst Size. A script was written for the Wavetek 395 that allowed the user to set ejection frequency, the number of droplets dispensed per trigger (burst sizes from 1 to 20 000 droplets), and the number of triggers for dispensing bursts into the microbalance (Table 1). The total mass of droplets dispensed was maintained above the minimum specification of the microbalance, which was determined to be well below 100 μg.[16] Three ejection frequencies were tested: 20 kHz, 5556 Hz, and 500 Hz. Fluidic pressure was held constant at −2.0 hPa. Each series of measurements was performed five times in randomized order, for a total of 285 mass determinations performed over several weeks. Average droplet mass was the measured burst mass divided by the number of droplets in a burst, and the differential droplet mass (for a burst of n droplets) was the mass difference between a burst of n droplets and a burst of $n - x$ droplets, with the difference divided by x. The differential mass may therefore be considered a mass estimate of the nth individual droplet.

RESULTS AND DISCUSSION

Dynamics of Droplet Formation. Some discussion on the droplet formation process is necessary to establish context for later explanations of observed droplet behaviors under variation in pulse frequency, fluidic pressure, and burst size. The process is highly complex, and theory regarding the underlying fluid dynamics and energetics governing droplet formation is far from resolved.[25−29] Using a storage oscilloscope and pulse counter, we confirmed that the DOD pulses driving the PZT device were simple trapezoidal waveforms without transients, overshoots, or ringing, and reproducible from the first to the last pulse requested. The amount of acoustic energy pumped into the fluid was therefore expected to be delivered continuously in discrete identical packets over the ejection duration. While interfacial tension, oscillations in droplet shape, viscoelastic forcing, and air friction account for significant energy loss,[30] a portion was manifested as kinetic energy (KE = $1/2mv^2$) of the droplet at the observation point 2.0 mm below the orifice. As a result, given a particular driving waveform and fluidic pressure, and in the absence of acoustic resonances, each droplet was expected to possess the same KE with partitioning between mass and velocity predicated by factors acting within the PZT device. Droplets ejected at resonance maxima would exhibit enhanced KE mainly from decreased viscoelastic dissipation within the acoustic cavity, and the energy budget from this source could be approached by systematic evaluation of the resonance profile.

Droplet Characteristics versus Ejection Frequency. Profiles of IBA droplet mass, velocity, and derived KE versus ejection period (and frequency) are exhibited in Figure 3, where data were obtained using a single driving waveform and a constant fluidic pressure. The variations in droplet velocity and mass were substantial: velocities ranged from 0.75 to 8.36 m/s, while masses varied from 42 to 130 ng. The three plots in Figure 3 are similar in their correlated display of resonance behavior at the higher frequencies (from 24 to about 3 kHz) and their relative flatness below 3 kHz. We identify three regions in these profiles that are delineated by IBA droplet formation characteristics: (1) the resonant region; (2) the transitional region; and (3) the quiescent region. Each is described in turn.

The Resonant Region. Droplets formed between 24 and 3 kHz were subject to strong acoustic resonances that created significant peaks in the droplet mass and velocity profiles (Figure 3), consistent with earlier reports.[14,17] The sequence of resonance peaks, with pulse cycle periods at 310, 260, 210, 155, 100, and 48 μs, occurred at regular intervals, and showed geometric growth in droplet KE where the increase above the baseline (about 0.1 nJ) approximately tripled at each step in the sequence. The highest droplet KE observed was 3.7 nJ. This suggests that, in the absence of resonance, less than 3% of the acoustic energy imparted by the PZT was manifested in the KE of the emerging droplet. The remainder was lost through interfacial friction and viscoelastic forcing as the acoustic waves propagated back and forth along the cavity; after about 18 L/c (340 μs), the residual waves became insignificant. However, if another pulse was delivered synchronously before 340 μs, the residual wave was captured and manifested in the KE of the successor droplet. The resultant KEs of the droplets became geometrically greater at shorter periods because fewer cavity transverses occurred and

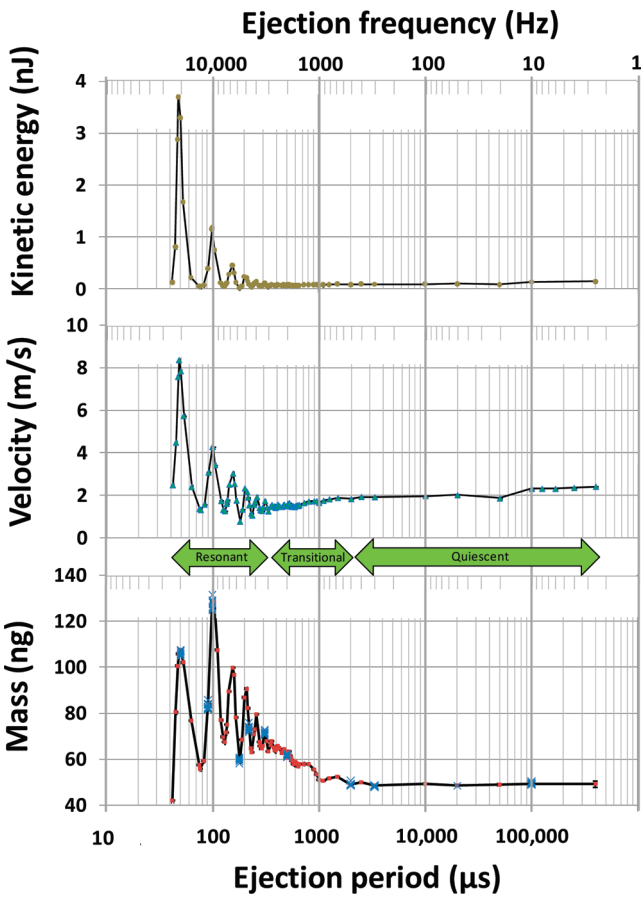

Figure 3. Characteristics of IBA microdrops across ejection cycle periods from 42 μs to 400 ms (ejection frequencies from 24 kHz to 2.5 Hz, top scale) using a single driving waveform and constant fluidic pressure. Droplet formation characteristics demarcate three regions: resonant (24 kHz to 3 kHz); transitional (3 kHz to 500 Hz); and quiescent (<500 Hz). Short-term analytical imprecision (standard deviation) is within the size of the markers. Long-term reducibility for each characteristic was measured at selected ejection periods noted by multiple crosses on the mass plot. See text for further description.

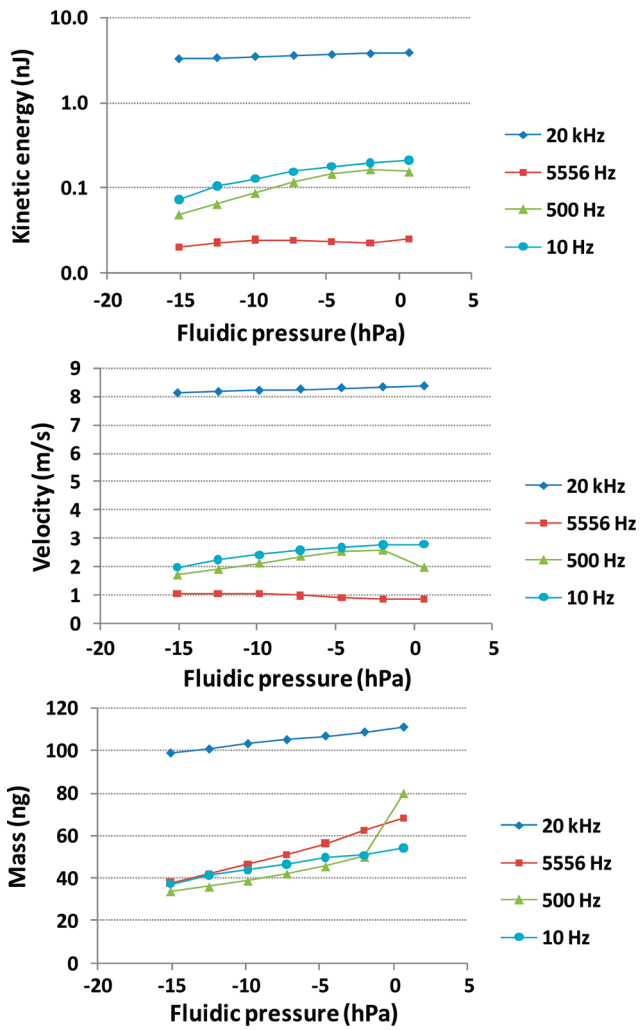

Figure 4. Sensitivity of IBA droplet mass, velocity, and kinetic energy to fluidic pressure at four ejection frequencies. Uncertainties are within the sizes of the data markers.

because the successor waves became compounded. The antiresonant (valley) periods of 235, 180, 125, and 75 μs also displayed periodic consistency. In our PZT device, resonances and antiresonances occurred with an average periodicity of 53 μs, which is in agreement with the expected of periodicity of 3 L/c or 54 μs (Figure 2). While the resonance peaks for mass and velocity were strongly associated, their values across the resonant region were only fairly correlated (Pearson's $r = +0.69$) because of underlying mass−velocity partitioning. This partitioning may be observed in the mass and velocity baselines, the values of which are negatively correlated (Pearson's $r = -0.80$).

The Transitional Region. Between 3 kHz and 500 Hz, the resonance peaks were dampened and difficult to distinguish (Figure 3). The KE profile was flat, while mass and velocity profiles were negatively correlated (Pearson's $r = -0.68$). Broad peaks were evident in the mass profile. The partitioning of mass and velocity within this region implies the influence of factors that act within 2 ms of droplet emergence and favor faster droplet velocities at longer ejection periods. There are several possibilities: patterns of capillary ripples[31] on the meniscus, refill effects from progressive migration of the meniscus into the orifice,[32] and triboelectric charging/discharging[33] of the nozzle within this time frame may be responsible for the observations. While intriguing, systematic exploration of these factors was beyond the scope of this study.

The Quiescent Region. Droplets that were formed at frequencies between 500 and 20 Hz were indistinguishable from each other; the characteristic profiles were flat (Figure 3). The droplet KE was approximately 0.1 nJ, amounting to less than 3% of the maximum KE displayed in the resonant region. Curiously, at ejection frequencies of 10 Hz and below, droplet velocity was observed to increase by about 20% without a change in mass. Oscilloscope comparisons of the driving waveforms indicated no differences, so we conclude that the quiescent domain may be influenced by factors that act over time scales greater than 2 ms; these may include convective fluid evaporation[34] with orifice dewetting and residue deposition. Droplets emerging at 10 Hz and below in fact behaved like first-drops generated at any frequency, which will be discussed in a later section.

Droplet Characteristics versus Fluidic Pressure. Profiles of droplet mass, velocity, and derived KE against fluidic pressure at four continuous ejection frequencies are exhibited in Figure 4. The frequencies were selected to represent different regions and

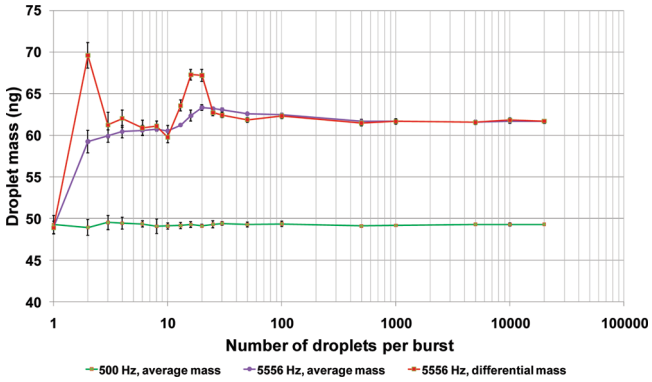

Figure 5. Profiles of average and differential droplet mass ejected at 5556 and 500 Hz as a function of burst size. Fluid was isobutanol ejected from a PZT device using a single waveform and a constant fluid pressure. Error bars are expanded uncertainties about the means of replicated measurements.

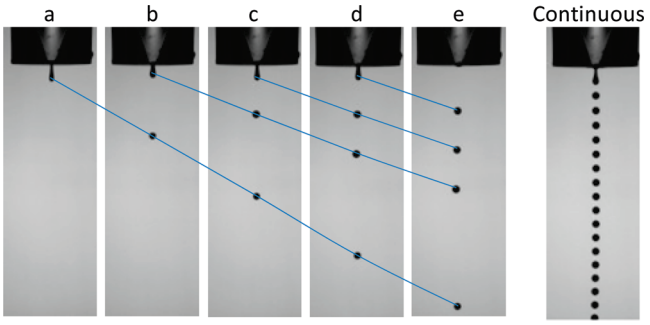

Figure 6. Images of IBA droplets ejected at 5556 Hz. Images a−e depict a four-droplet burst sequence, with each image separated in virtual time by 180 μs, the ejection cycle period. Lines were added to identify a particular droplet across the sequence. Because 5556 Hz is an antiresonance frequency, the first droplet traveled at a greater velocity than the following droplets, which eventually reached a minimum steady-state velocity as depicted by the continuous ejection image at right. This steady-state condition required continuous ejection of at least 100 droplets as measured by mass; see Figure 5.

conditions within the frequency profile: resonant (20 kHz), antiresonant (5556 Hz), transitional/quiescent (500 Hz), and quiescent (10 Hz). The smallest and largest KEs were characteristic of droplets ejected at 5556 Hz and 20 kHz, respectively, and the 5556 Hz profile was essentially flat. The 10 Hz, 500 Hz, and 20 kHz profiles exhibited increases as fluidic pressure increased. The mass profile (bottom plot) exhibited fairly linear trends in droplet size as fluidic pressure increased and showed nonlinear behavior for the 500 Hz ejections at the highest pressure. There, droplet mass increased 60% from the mass measured at the neighboring pressure level. This behavior was also observed at 300 Hz (data not shown), but not at 10 Hz, 5556 Hz, or 20 kHz. At the highest pressure, the fluid meniscus was observed to protrude slightly from the orifice between droplet ejections, which for 500 Hz (and 300 Hz) interfered strongly with the continuous ejection process. At the same high pressure, droplet velocity significantly decreased (middle plot), while the KE of these droplets was somewhat less than expected from the trend indicated by the other pressures. We noticed large oscillations within these large droplets, indicating significant capillary forces and surface energy that could help explain the anomaly.

Droplet Characteristics versus Burst Size. Profiles of average and differential droplet mass versus the number of droplets in a burst are displayed in Figure 5 for two frequencies representing different ejection conditions. The monotonic profile for ejections at 500 Hz indicates that the average and individual droplet masses in any burst were equal, which was expected in the quiescent region. The profiles for ejections at 5556 Hz, an antiresonant point, showed significant nonlinear mass effects. The first droplet in any burst had a mass of 48 ng and represented the minimum droplet mass, whereas the second droplet mass was about 69 ng and larger than all subsequent droplets. Masses then decreased to about 60 ng at the 10th droplet (1.8 ms), then increased again to about 67 ng at the 20th droplet (3.6 ms). Afterward, droplet mass decreased and established a steady-state mass of 62 ng after dispensing about 50 droplets (9 ms). It may be expected that the fluidic pressures within the PZT device initially increase, out of equilibrium with the reservoir headspace pressure, as the driving waveform pumps energy into the fluid. Next, as the fluidic pressure re-equilibrates, perhaps as an oscillation damped by viscoelastic forces, droplet mass would approach a steady state. This would explain the relatively large droplets ejected after the first droplet in the resonant region, as well as the echo in the profile. The amount of pressure oscillation responsible for the 10 ng variation displayed in Figure 5 would amount to about 10 hPa peak-to-peak, which is reasonable considering that the baseline fluidic pressure operating range is over 15 hPa (Figure 4).

Figure 6 displays the images of a 4-droplet burst ejected at 5556 Hz. Because of antiresonant droplet formation, which influences all but the first droplet, the velocities of subsequent droplets slow until eventually reaching the continuous ejection state depicted on the image at right. Droplet velocity during the manifestation of the pressure oscillation was expected to exhibit only a monotonic profile because velocity was found to be fairly insensitive to fluidic pressure at 5556 Hz (Figure 4). This was indeed the case, as velocity measurements of the second to 20th droplet showed only a gradual decrease in velocity. The diameter of the second droplet was about 13% larger than the first droplet, in agreement with the mass measurements. Optical resolution limitations (1.1 μm/pixel, equivalent to 4 ng/droplet) precluded a meaningful comparison of the subsequent individual droplets, which ranged between 67 and 60 ng in mass.

Figure 7 shows nonlinear 20 kHz mass data for burst sizes from 1 to 20 000 droplets. The first droplet had a mass of 48 ng, the second reached 68 ng, and the third ejection had a surprisingly large mass of 145 ng. The masses of subsequent droplets decreased to about 93 ng and then gradually increased to the steady-state droplet mass of 102 ng after about 100 droplets (5 ms). This process was visualized on the video system for bursts of 2, 3, and 5 droplets (Figure 8). The 2-drop burst showed the first droplet quickly overtaken by the second larger droplet and followed by a slower satellite. Some excess fluid emerged after the 2-drop burst but was reabsorbed into the orifice. This was not the case for the 3-drop and 5-drop bursts (and presumably all bursts ≥ 3 droplets in the resonant region), where excess fluid was ejected at the end of the burst. These postburst ejecta are most likely a result of some residual acoustic waves having sufficient energy during viscoelastic ring-down. The postejecta caused the derived differential mass of the third drop to be inflated as observed in Figure 7, and subsequent ($n > 3$) estimations of differential mass did not entirely compensate for this effect because the amount of postejecta was not constant; some variation in postejecta for the 3-drop and

5-drop bursts is visualized in Figure 8. Data in Figure 7 suggest that the amount of postejecta had stabilized for bursts where n was greater than 10; yet for n between 30 and 100 the droplet mass increased by about 10% to a steady state. As was proposed for the 5556 Hz observations, this change could be explained by the presence of a damped pressure oscillation brought on by the initial pressure spike reflected in the third ejection, which re-equilibrated and reached the steady-state droplet mass only after about 100 droplets had passed (5 ms). The corresponding changes in droplet velocity could not be effectively measured because, at 20 kHz, the relatively slow first droplet was impacted by several subsequent drops within the 2 mm distance from the orifice needed for optical measurement (Figure 8).

Reproducibility of Droplet Mass and Velocity Measurements. The long-term reproducibilities of droplet size and velocity were determined at ejection frequencies representing several types of dispensing conditions. Table 2 summarizes gravimetric and optical measurements taken across several weeks. As one may expect, mass reproducibilities were marginally better when dispensing droplets in the quiescent region. Mass variations ranged from 0.6% (for a 5-drop burst dispensed at 500 Hz) to 1.3% (for a 5000-drop burst dispensed at 10 Hz). Surprisingly, for dispense conditions on steep slopes in the mass profile midway between resonant and antiresonant peaks (condition "S" in Table 2), variations were only 1.4−1.6%. The 1.6% value was matched when dispensing at 10 kHz, a resonant peak where the largest droplets were formed. The standard deviations in the optical measurements of droplet velocity ranged from 0.02 to 0.05 m/s, with the latter associated with ejections at 10 Hz. Their relatively high standard deviation is attributed to variations in interfacial forces at the orifice during formation of these "first-droplets", which possess the highest velocities in the quiescent region.

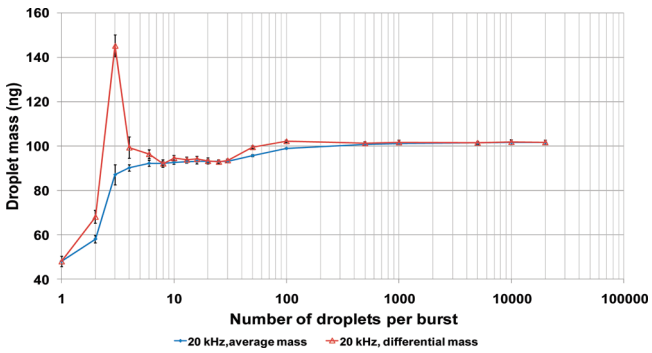

Figure 7. Profiles of average and differential droplet mass ejected at 20 kHz as a function of burst size. Fluid was isobutanol ejected from a PZT device using a single waveform and a constant fluid pressure. Error bars are expanded uncertainties about the means of replicated measurements.

Uncertainty Evaluation. The uncertainties in the values of droplet (or burst) mass m, derived from gravimetric measurements, are expressed as either a standard combined uncertainty (u_c) or a relative combined uncertainty (u_c/m), and are determined according to the ISO/IEC and NIST Guides.[35] Values of u_c are intended to represent, at the level of one standard deviation, the combined effects of gravimetric imprecision, microbalance calibration uncertainty, and irreproducibility in dispense conditions leading to variations in droplet size. Gravimetric imprecision was determined empirically for each method as previously outlined, and ranged from 0.2% to 0.5% depending on method and aliquot amount. Microbalance uncertainty for differential mass measurements, after testing with standard weights, was 0.1%.

Our ability to measure the fluidic pressure was limited mainly by the measurement resolution of the h value (±0.1 mm), whereas variation in the regulated headspace pressure amounted to ±0.02 hPa. Together, these corresponded to an uncertainty in fluidic pressure of 0.10 hPa, which we found translated to a typical

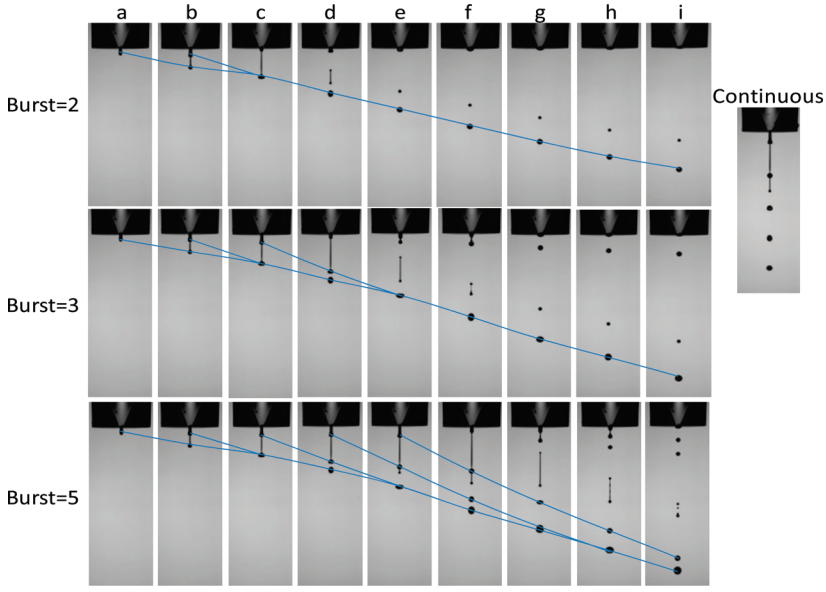

Figure 8. Images of IBA droplets ejected at 20 kHz. Each row of images depicts a 2-droplet, 3-droplet, or 5-droplet burst sequence, with each image separated in time by 50 μs, the ejection period. Lines were added to identify a particular droplet across each sequence. Note that the 2-droplet burst includes a satellite from the last droplet, while the 3-droplet and 5-droplet bursts include a satellite plus superfluous ejecta emerging after the last droplet. Because 20 kHz is a resonance frequency, the first droplet traveled at a slower velocity than did the following droplets, which overtook and coalesced with that droplet. The steady-state condition is depicted by the image at right, which was reached after continuous ejection of about 100 droplets as measured by mass; see Figure 7.

Table 2. Gravimetric and Optical Results of Isobutanol Droplet Analyses

		gravimetry			optical analysis	
ejection frequency (Hz)	dispense condition[a]	burst size (no. droplets × no. repeats)	average droplet mass (ng)	long-term variation (RSD)	average droplet velocity (m/s)	long-term variation (sd, m/s)
10	Q	5000 × 1	49.3	1.3% (n = 13)	2.31	0.05 (n = 9)
300	Q	20 000 × 1	48.1	0.7% (n = 13)	1.87	0.03 (n = 10)
500	Q–T	20 000 × 1	48.9	1.0% (n = 21)	1.78	0.03 (n = 12)
2000	T	20 000 × 1	61.2	1.1% (n = 14)	1.48	0.03 (n = 9)
3226	R	20 000 × 1	71.4	1.2% (n = 13)	1.65	0.02 (n = 9)
4545	S	20 000 × 1	73.5	1.4% (n = 13)	1.56	0.05 (n = 9)
5556	A	20 000 × 1	59.8	1.4% (n = 13)	0.77	0.02 (n = 9)
10 000	R	20 000 × 1	127.4	1.6% (n = 14)	4.22	0.02 (n = 9)
10 989	S	20 000 × 1	82.8	1.6% (n = 14)	2.90	0.04 (n = 9)
20 000	R	20 000 × 1	106.3	0.8% (n = 13)	7.63	0.03 (n = 9)
500	Q–T	5 × 1000	48.8	0.6% (n = 6)		
20 000	R	5 × 1000	95.7	0.9% (n = 8)		

[a] Q, quiescent; T, transitional; A, antiresonant; S, slope; R, resonant.

droplet mass uncertainty of 0.10 ng. This source of variation did not affect the short-term repeatability of droplet size but applied to mass measurements upon reset of static head or reservoir head pressure, such as after a fluid purge through the dispense device. Because most DOD procedures require fluid purges on occasion, fluid pressure uncertainty has been included in all reported combined standard uncertainties.

CONCLUSIONS

Using both gravimetric and optical measurements, operational factors are shown to influence, quantitatively and consistently, the mass and velocity of droplets emerging from a DOD dispenser. The growth of air bubbles within the dispensing device may be easily monitored and avoided. A droplet burst of any number may be reproducibly dispensed (within 1.6% RSD) at any viable ejection frequency, and the mass per droplet can be varied considerably (here, from 40 to 130 ng) by selecting specific operating conditions. The relationship between droplet mass and ejection frequency is dominated by predictable acoustic resonance effects at frequencies greater than 3000 Hz. Between 3000 and 500 Hz, acoustic resonances are subdued and replaced by factors that partition the mass and velocity of the emerging droplets while maintaining their initial KE. At ejection frequencies less than 500 Hz, droplet formation occurs under stable quiescent conditions, although droplet velocity increases by 10% for ejections at and below 10 Hz, where "first drops" are essentially produced. The first-drop issue is resolved in profiles that plot average and differential droplet mass versus burst size. At 500 Hz, the profile is flat, indicating consistency of mass across all droplets in a burst of any size. At resonant frequencies, nonlinear mass effects are observed in individual droplets up through the 100th droplet. Postburst ejecta are observed, likely from residual acoustic energy during ring-down. The development of high-throughput applications that require accurate dosing at high rates of ejection must compensate for these effects.

ASSOCIATED CONTENT

Supporting Information. (I) The reservoir headspace pressure control system; (II) reproducibility of isopropanol printing; (III) validation of eq 1; and (IV) attenuation of droplet velocity by air resistance. This material is available free of charge via the Internet at http://pubs.acs.org.

AUTHOR INFORMATION

Corresponding Author
*E-mail: r.verkouteren@nist.gov.

ACKNOWLEDGMENT

We gratefully acknowledge the Science & Technology Directorate of the U.S. Department of Homeland Security and the NIST Office of Law Enforcement Standards for sponsoring this work. We also wish to acknowledge Dr. Hans Jochen Trost of MicroFab Technologies for valuable discussions during preparation of this manuscript.

REFERENCES

(1) Theberge, A. B.; Courtois, F.; Schaerli, Y.; Fischlechner, M.; Abell, C.; Hollfelder, F.; Huck, W. T. S. *Angew. Chem., Int. Ed.* **2010**, *49*, 5846–5868.
(2) Tarcha, P. J.; Verlee, D.; Hui, H. W.; Setesak, J.; Antohe, B.; Radulescu, D.; Wallace, D. *Ann. Biomed. Eng.* **2007**, *35*, 1791–1799.
(3) Hoth, C. N.; Schilinsky, P.; Choulis, S. A.; Brabec, C. J. *Nano Lett.* **2008**, *8*, 2806–2813.
(4) Guillotin, B.; Guillemot, F. *Trends Biotechnol.* **2011**, *29*, 183–190.
(5) Wang, S.; Ang, P. K.; Wang, Z.; Tang, A. L. L.; Thong, J. T. L.; Loh, K. P. *Nano Lett.* **2010**, *10*, 92–98.
(6) Kang, H. R. *J. Imaging Sci.* **1991**, *35*, 195–201.
(7) Dong, H.; Carr, W. W.; Morris, J. F. *Rev. Sci. Instrum.* **2006**, *77*, 085101.
(8) Famili, A.; Palkar, S. A.; Baldy, W. J., Jr. *Phys. Fluids* **2011**, *23*, 012109.
(9) Eggers, J.; Villermaux, E. *Rep. Prog. Phys.* **2008**, *71*, 036601.
(10) Eggers, J. *Rev. Mod. Phys.* **1997**, *69*, 865–929.
(11) Lee, E. R. *Microdrop Generation*; CRC Press LLC: Boca Raton, FL, 2003.
(12) Wijshoff, H. *Phys. Rep.* **2010**, *491*, 77–177.
(13) Chen, A. U.; Basaran, O. A. *Phys. Fluids* **2002**, *14*, L1–4.
(14) Technical Notes No. 99-04, Orifice Diameter Effects; Microfab Technologies Inc.: Plano, TX, 1999; http://www.microfab.com/equipment/technotes/technote99-04.pdf.

(15) Jang, D.; Kim, D.; Moon, J. *Langmuir* **2009**, *25*, 2629–2635.
(16) Verkouteren, R. M.; Verkouteren, J. R. *Anal. Chem.* **2009**, *81*, 8577–8584.
(17) Bogy, D. B.; Talke, F. E. *IBM J. Res. Dev.* **1984**, *28*, 314–321.
(18) Technical Notes No. 99-03, Drive Waveform Effects on Ink-jet Device Performance; Microfab Technologies Inc.: Plano, TX, 1999; http://www.microfab.com/equipment/technotes/technote99-03.pdf.
(19) Satellites Occurrence and Approaches to Eliminate Them; MicroFab Technologies Inc.: Plano, TX, 2007; http://www.microfab.com/equipment/technotes/Satellites_version_09_26_07.pdf.
(20) de Jong, J.; de Bruin, G.; Reinten, H.; van den Berg, M.; Wijshoff, H.; Versluis, M.; Lohse, D. *J. Acoust. Soc. Am.* **2006**, *120*, 1257–1265.
(21) Brennen, C. E. *Cavitation and Bubble Dynamics*; Oxford University Press: New York, 1995; Chapter 1.
(22) Hine, N. P. *J. Imaging Technol.* **1991**, *17*, 223–227.
(23) Antohe, B. V.; Wallace, D. B. *J. Imaging Sci. Technol.* **2002**, *46*, 409–414.
(24) Troncoso, J.; Carballo, E.; Cerdeiriña, C. A.; González, D.; Romaní, L. *J. Chem. Eng. Data* **2000**, *45*, 594–599.
(25) Trinh, E. H.; Thiessen, D. B.; Holt, R. G. *J. Fluid Mech.* **1998**, *364*, 253–272.
(26) Ardekani, A. M.; Sharma, V.; McKinley, G. H. *J. Fluid Mech.* **2010**, *665*, 46–56.
(27) Morrison, N. F.; Harlen, O. G. *Rheol. Acta* **2010**, *49*, 619–632.
(28) Minale, M. *Rheol. Acta* **2010**, *49*, 789–806.
(29) Castrejón-Pita, J. R.; Morrison, N. F.; Harlen, O. G.; Martin, G. D.; Hutchings, I. M. *Phys. Rev. E* **2011**, *83*, 036306.
(30) Megias-Alguacil, D. *J. Colloid Interface Sci.* **2007**, *314*, 251–255.
(31) Westra, M.-T.; Binks, D. J.; Water, W. *J. Fluid Mech.* **2003**, *496*, 1–32.
(32) Balasubramaniam, R.; Subramanian, R. S. *Ann. N. Y. Acad. Sci.* **2004**, *1027*, 303–310.
(33) Kim, O. V.; Dunn, P. F. *Aerosol Sci. Technol.* **2010**, *44*, 292–301.
(34) Iorio, C. S.; Goncharova, O.; Kabov, O. A. *Microgravity Sci. Technol.* **2009**, *21*, S313–S319.
(35) International Organization for Standardization. *Guide to the Expression of Uncertainty in Measurement (ISO-GUM)*; Geneva, Switzerland, 1993; ISBN 92-67-10188-9. See also: Taylor, B. N.; Kuyatt, C. E. *Guidelines for Evaluating and Expressing Uncertainty of NIST Measurement Results*; NIST Technical Note 1297, U.S. Government Printing Office: Washington, DC, 1994; available at http://physics.nist.gov/pubs/.